5th International Conference on Experimental Fluid Mechanics – ICEFM 2018 Munich
Munich, Germany, July 2-4, 2018

Effects of the configuration characteristics on the motion parameters of autorotating flight of plant seeds

Myong H Sohn[1]*

[1] Cheongju University, Department of Aeronautical and Mechanical Engineering,
Cheonju, Republic of Korea
*myongsohn@cju.ac.kr

Abstract

The present study investigates the effect of the configuration characteristics on the motion parameters of the autorotating flight of plant seeds. The 3D geometry of sample plant seeds was obtained using synchrotron X-ray micro-CT, and their motion parameters were measured. Numerical simulation was then carried out based on the real 3D seed geometry and motion parameters measured. It was found that a compact leading edge vortex (LEV) was developed over the leeward surface of the seed blade, and the spanwise vorticity inside the LEV was transported into the tip-passing wake via strong spanwise velocity. This behavior of LEV was in congruence with the previous experimental study for the artificial maple seeds in autorotating flight. The interrelation between the 4 motion parameters of the autorotating flight of plant seeds (descent speed, spinning rate, coning angle and pitch angle) was also investigated through the sensitivity study of the motion parameters.

1 Introduction

The flight of plant components is carried out through the fixed configuration, which is different from the wings of birds and insects. The present study investigates the effect of the plant seeds' configuration characteristics on the motion parameters of the autorotating flight of plant seeds. The 3D geometry of sample plant seeds was obtained using synchrotron X-ray micro-CT, and their motion parameters were measured. Numerical simulation was then carried out based on the real 3D seed geometry and motion parameters measured. The sensitivity study of the motion parameters (the pitch angle, the coning angle and the advance ratio) was also performed to investigate the effect of them on the aerodynamic force and torque generation, and the interrelation between the motion parameters for the autorotating flight of plant seeds.

Autorotation is the result of a delicate equilibrium between gravity (weight of the seed) and inertial as well as aerodynamic forces. In the steady vertical flight of an autorotating seed, the vertical component of aerodynamic force and the weight of the seed are balanced, as are the resistant and driving torques. Figure 1 shows the forces and the motion parameters of autorotation. Even in the vertical descent of an autorotating seed, the seed blade plane is not perpendicular to the vertical spinning axis. The tangent plane to the conical surface swept by the seed blade (flight path plane in this study) makes an angle β with the horizontal plane, and this angle is defined as the coning angle (Fig. 1a). The coning angle ranges from 15° to 30° for maple seeds (Azuma and Yasuda, 1989). The angle between the flight path plane and the chord line of the blade is called as the pitch angle θ (Fig. 1b). The positive direction of the pitch angle is defined as the nose-up direction in the present study. The pitch angle of maple seeds is usually small, within the range of 2° (Azuma and Yasuda, 1989). The flight path plane makes an angle of $\tan^{-1}(V_D\cos\beta/r\Omega)$ with the resultant relative wind that is the vector sum of the rotational velocity ($V_H = r\Omega$) and the descent velocity component ($V_D\cos\beta$). This angle is represented by φ in Fig. 1b. Therefore, the local angle of attack α of the local blade section becomes $\varphi+\theta$.

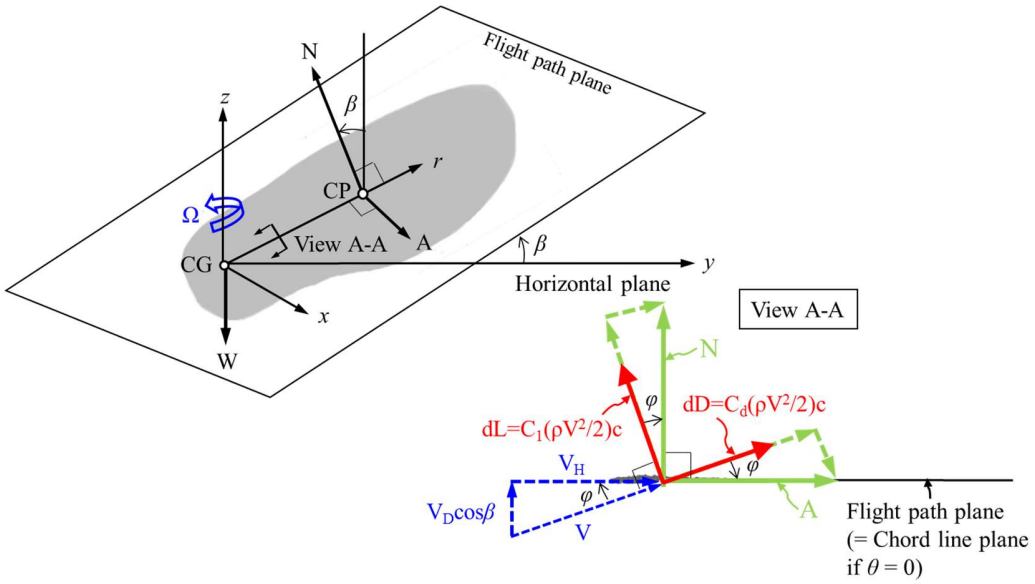

Figure 1 : Forces and motion parameters of autorotation. x is the flapping axis; r is the span coordinate; z is the spinning axis; W, weight of the seed; N, normal force component of the resultant aerodynamic force; A, axial force component of the resultant aerodynamic force; dL, sectional lift; dD, sectional drag; CG, center of gravity; CP, acting point of the resultant aerodynamic force; β, coning angle; Ω, spinning rate; θ, pitch angle; V_D, descent velocity; V_H, horizontal velocity due to rotation ($r\Omega$); V, effective wind velocity; φ, $\tan^{-1}(V_D\cos\beta/V_H)$; α, local angle of attack ($\varphi+\theta$).

2 Experimental and Numerical Procedures

2.1 Measurement of Sample Seed Geometry and Motion Parameters

Sample seeds in a natural fallen condition were collected in Mid-October and November, and they were preserved in a plastic box sealed with paraffin to conserve their water content. The mass of the sample seeds was measured just before the experiment using an electronic balance (OHAUS AP2500 Analytical Plus; accuracy=0.01 mg). The span, chord, and planform area of the sample seeds were measured using enlarged photo images. Synchrotron X-ray micro-CT was employed to obtain the 3D morphological structures of the sample seeds, such as surface roughness and section geometry. Tomographic 3D images were reconstructed from the sliced images.

The motion parameters of autorotative flight of sample seeds were measured using a high-speed camera (Photron Fastcam Ultima APX). Free-fall tests were performed in a closed chamber to avoid any disturbance by surrounding wind. The seeds were released from 2 m above the floor of the test chamber. The distance between the first and last images of the stable autorotating flight was calculated by counting the pixel numbers between the images. The accuracy of this distance calculated was checked by the vertically mounted reference scale. The time elapsed between the first and last images was calculated by counting the number of images involved (usually ~200 images) with the frame speed used to record images consecutively (1000 frames/s). Then the descent velocity was obtained by dividing the distance with the time elapsed. The average of 5 measured descent velocities was 1260±48.1 mm/s (mean±standard deviation).

For the measurement of spinning rate, two images captured at the same phase were selected among the instantaneous images showing the falling trajectory of each seed. The time elapsed for one revolution was calculated from the number of frames between the two images. The average spinning rate of the 5 measurements was approximately 133.6±10.4 rad/s. Several images were selected among the consecutive instantaneous images for a maple seed to measure the coning angle β, and they were overlapped to have the same axis of rotation. The coning angles measured from the overlapped images were then averaged to obtain the representative coning angle. The average coning angle for 5 measurements was approximately 19.4°±2.5°. The pitch angle was not measured due to its small value and set to be zero.

2.2 Numerical Simulation

A 3D incompressible flow was numerically simulated using a commercial solver (STAR-CCM+). The second-order upwind scheme was used in numerical discretization. The following are the governing equations used in this study.

$$\nabla \cdot \left(\rho \vec{v} \right) = 0 \tag{1}$$

$$\frac{\partial}{\partial t}\left(\rho \vec{v} \right) + \nabla \cdot \left(\rho \vec{v}\vec{v} \right) = -\nabla p + \nabla \cdot \left(\overline{\overline{\tau}} \right) \tag{2}$$

where p is static pressure, $\overline{\overline{\tau}}$ is stress tensor.

The stress tensor $\overline{\overline{\tau}}$ is given by

$$\overline{\overline{\tau}} = \mu \left[\left(\nabla \vec{v} + \nabla \vec{v}^{T} \right) - \frac{2}{3} \nabla \cdot \vec{v} I \right] \tag{3}$$

where μ is the molecular viscosity and I is a unit tensor.

The polyhedral grids for numerical calculation was generated from the surface node data obtained from the 3D CT image of the sample seed using Star-CCM+. For accuracy, fine faces with edges length around 0.04 mm were constructed on seed surface. In order to resolve flow near the seed surface, 8 prism layers of 0.2 mm in total thickness with an incremental rate of 1.1 in thickness. The total number of grids was approximately 8,100,000. The spinning motion of the seed was implemented in the numerical simulation using multiple reference frame (MRF) method. The spinning rate was applied to the inner grids and descent velocity was applied to both of inner and outer grids.

3 Results and Discussion

3.1 Flow Pattern

Figure 2 shows the sectional streamlines, the spanwise vorticity distribution and the surface pressure distribution for the maple seed (*A. palmatum*), which is one of the most prevailing plant seeds taking autorotation wind dispersal. The motion parameters of the sample maple seed were 1.26 m/s for descent velocity, 133.6 rad/s for spinning rate, 19.4° for coning angle, and 0° for pitch angle. The flow separated at the leading edge and formed a shear layer of clockwise vorticity that developed into a large-scale leading edge vortex (LEV) attached over the leeward surface of the seed blade. This attached LEV causes a large negative (suction) pressure on the leeward surface of the seed blade, creating a high lift distribution. The suction pressure is dominant over the leeward surface of the seed blade. The largest suction pressure occurs in the narrow region near the leading edge, which reflects the seed morphology characterized by the thick leading edge and the corrugated surface due to the intense distribution of the thick vascular bundles.

Figure 3 shows the 3-dimensional flow structures, the spanwise velocity, and the spanwise transport of vorticity ($v \cdot \omega_r$). Fig. 3(a) shows that the spanwise-spiraling vortex flow is developed over the leeward surface of the seed blade. Tracer particles make spiral trajectories over the front part of the leeward surface and move toward the tips of the seed blade, and they merge with the tip-passing fluid particles making tip-trailing vortex. A spanwise flow is formed over the leeward surface of the seed blade (Fig.3(b)), and the spanwise transport of vorticity is peaked at the front part of the seed blade in the inner span positions (Fig. 3(c)). The spanwise flow and the spanwise transport of vorticity over the leeward surface of the seed blade observed in Fig. 3, are consistent with the results of the experimental study for the artificial maple seeds of Lentink et al. (2009). The spanwise-spiraling vortex flow and the spanwise transport of vorticity are considered as the key mechanism which makes the LEVs be stable and attached onto the seed surface even at very high angles of attack ($\alpha \approx 54°$ at 0.25R, $\alpha \approx 35°$ at 0.50R).

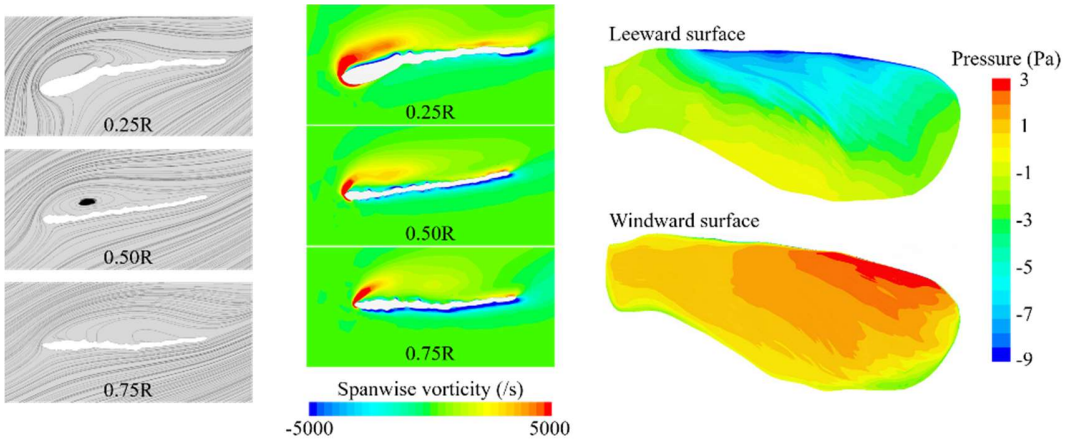

(a) (b) (c)

Figure 2 : Sectional streamlines (a), spanwise vorticity distribution (b) and surface pressure distribution (c) for *A. palmatum* maple seed

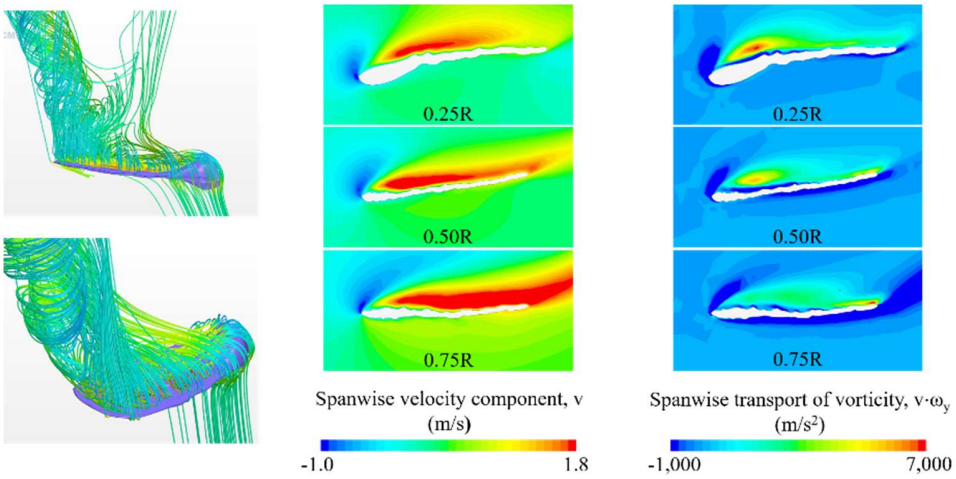

(a) (b) (c)

Figure 3 : Three-dimensional flow structure (a), spanwise velocity distribution (b), and spanwise transport of vorticity (c) for *A. palmatum* maple seed

3.2 Force and Torque

Figure 4 shows the sectional distributions of the normal force (N), the axial force (A), and the lift and drag coefficients. The normal force concentrates at outer span region and the axial force widely distributes along the span as shown in Fig. 4(a). The net axial force (accelerating force minus decelerating force) is positive (in the direction of rotation) and dominant in the inner span region. The main portion of the normal force comes from the suction pressure on the leeward surface of the seed, and the main source of the axial force is the shear stress acting the seed surface. Norberg (1973) calculated the aerodynamic forces employing the blade element theory for the samara of *Acer platanoides*, and reported that the sectional normal force was in the range of 7.3×10^{-2} N/m and the center of pressure was located at 0.66R with R as the turn radius. In the present study, the largest sectional normal force was in the range of 7×10^{-2} N/m and the largest sectional axial force was in the range of 3×10^{-2} N/m. The total normal force acted at 0.56R and the total axial force acted at 0.34R.

Fig. 4(b) shows the sectional lift and drag coefficient distributions. The sectional lift and drag coefficients are non-dimensionalized by the local chord and the local dynamic pressure, $0.5\rho[V_D^2+(r\Omega)]^2$. The normal force takes most of the sectional lift, whereas the normal and axial forces evenly contribute to the sectional

drag. The lift and drag coefficient exhibit maximum near the base of the seed and rapidly decrease toward the tip of the seed where the local dynamic pressure is large and the local chord is small. The maximum value of the lift coefficient was about 2.47 at about 0.22R position. The magnitude of the drag coefficient has the same order of magnitude of the lift coefficient, but less than that of the lift coefficient.

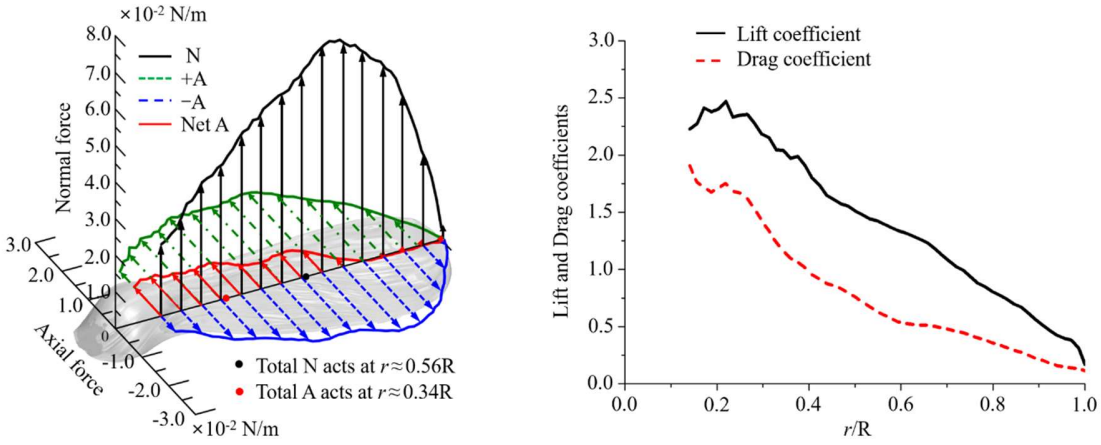

(a) (b)

Figure 4: Spanwise distribution of normal and axial forces (a), spanwise distribution of lift and drag coefficients (b) for *A. palmatum* maple seed

3.3 Sensitivity Study for Motion Parameters

The autorotating flight of plant seeds has self-stability and this is accomplished entirely through the structural pattern of the seeds as pointed out by Norberg (1973). The plant seeds taking the autorotation type of wind dispersal enter into the stable phase of autorotational descent with almost constant descending speed and spinning rate after some transient phases. There are 4 motion parameters in the autorotating flight of plant seeds, the descent speed, the spinning rate, the coning angle, and the pitch angle. These 4 motion parameters change during the transient phases of autorotational descent, and this change is interacted. For example, if the spinning rate increases, the coning angle decreases due to the increase of the centrifugal force, and the descent speed decreases because the upward vertical component of the aerodynamic force generated by the seed blade increases. The interaction of the motion parameters is investigated through the sensitivity study for the motion parameters.

Figure 5(a) shows the spinning torque variation with the pitch angle. The spinning torque rapidly decreases as the pitch angle increases from -5° to 5° (Natural maple seeds have the pitch angles in the range of -2° to 0°). In the present study, the positive pitch angle is defined as the nose-up direction. The spinning torque is dissected into the accelerating, the decelerating, and the net torque variation along the span as shown in Fig. 5(b). Fig. 5(b) shows that the accelerating torque increases as the pitch angles increases. However, the increase rate of the decelerating torque is larger than that of the accelerating torque, and then the net spinning torque decreases as the pitch angle increases.

By employing the notation of Fig. 1, the infinitesimal driving torque generated by dr becomes $(\mathrm{dL}\sin\varphi)(dr)(r)$, whereas he infinitesimal resisting torque generated by dr becomes $(\mathrm{dD}\cos\varphi)(dr)(r)$. dL denotes the lift component acting on the blade section of infinitesimal span dr, and dD is the drag component acting on dr. The total spinning torque to drive the rotation about the z-axis is obtained by integrating the net infinitesimal torque $[(\mathrm{dL}\sin\varphi) - (\mathrm{dD}\cos\varphi)](\cos\beta)rdr$ over the whole seed blade. The spinning rate becomes steady when this total spinning torque becomes zero as follows.

$$\int_{r=-R_b}^{r=R_t} (\mathrm{dL}\sin\varphi - \mathrm{dD}\cos\varphi)\, r\cos\beta\, dr = 0$$

where the upper limit of the integration (R_t) is the distance between the spinning axis of autorotation and the wing tip of the seed and R_b is the distance between the spinning axis and the base tip of the seed.

Therefore, it can be concluded that the rapid decrease of the spinning torque for the positive pitch angle is due to the increase of the decelerating spinning torque dominated by the increase of the drag component of the resultant aerodynamic force. The effect of the other motion parameters (the descent speed, the spinning rate and the coning angle), and the effect of them on the aerodynamics force and torque generation, and the interrelation between these motion parameters were also investigated.

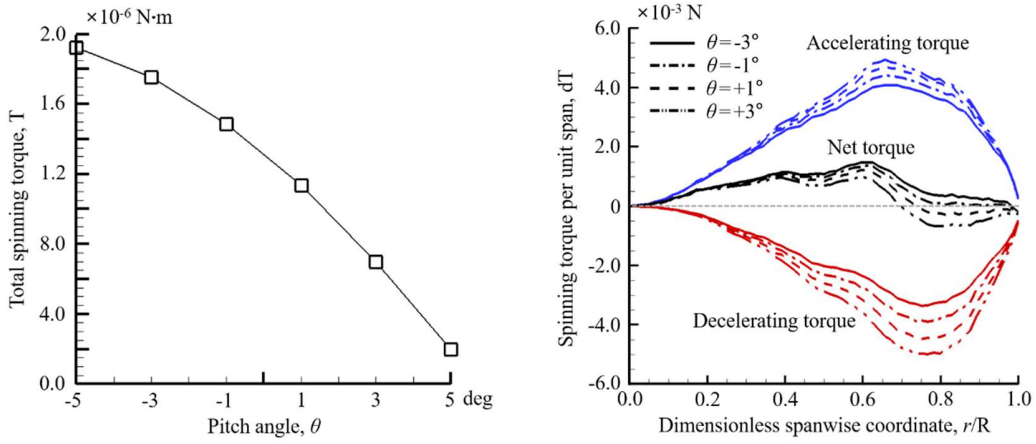

Figure 5 : Total spinning torque variation with pitch angle (a), spanwise distribution of accelerating, decelerating and net spinning torque with pitch angle (b) for *A. palmatum* maple seed

4 Conclusion

The effect of the configuration characteristics on the motion parameters in the autorotating flight of plant seeds was investigated though the combined experimental and numerical study. The present study revealed the unique aerodynamic features of the autorotating flight of plant seeds, such as the large suction pressure distribution on the leeward surface of the seed blade, the stable leading edge vortex formation in the leeward region over the seed, and the aerodynamic force distribution along the span of the seed blade. The sensitivity study of the motion parameters of the autorotating flight of plant seeds was performed. The spinning torque rapidly decreases as the pitch angle increases in the positive direction (nose-up direction), and this is due to the increase of the drag component of the resultant aerodynamic force. Among the 4 motion parameters (descent speed, spinning rate, coning angle and pitch angle), the pitch angle was found to be the most influential one.

Acknowledgements

This research was supported by Basic Science Research Program through the National Research Foundation of Korea (NRF) funded by the Ministry of Science, (NRF-2016R1A2B1015).

References

Azuma A and Yasuda K (1989) Flight performance of rotary seeds. *J. Theo. Biol.* 138 : 23-53.

Lentink D, Dickson W B, van Leeuwen J L, and Dickinson M H (2009) Leading edge vortices elevate lift of autorotating plant seed. *Science* 324 : 1438-1440.

Norberg R A (1973) Autorotation, self-stability, and structure of single-winged fruits and seeds (samaras) with comparative remarks on animal flight. *Biol. Rev.* 48 : 561-596.